



Transcriptomic analysis of cells in response to EV71 infection and 2A^{pro} as a trigger for apoptosis via TXNIP gene

Chenguang Yao¹ · Kanghong Hu¹ · Caili Xi¹ · Ni Li¹ · Yanhong Wei¹

Received: 25 May 2018 / Accepted: 30 October 2018
© The Genetics Society of Korea and Springer Nature B.V. 2018

Abstract

Background Enterovirus 71 (EV71) is the main pathogen of hand-foot-mouth disease (HFMD) and sometimes causes several neurological complications. However, the underlying mechanism of the host response to the virus infection remains unclear.

Objective To reveal the cell-specific transcriptional response of cultured RD cells following infection with EV71, and better understand the molecular mechanisms of virus-host interactions.

Methods The RD cells were infected with or without EV71 for 24 h, and then transcriptome sequencing and qRT-PCR were performed to analyze the transcriptome difference of functional genes.

Results More than 15000 genes were identified in transcriptome sequencing. In comparison with uninfected RD cells, 329 DEGs were identified in cells infected with EV71. GO and KEGG pathway enrichment analysis showed that most of the DEGs were related to DNA binding, transcriptional regulation, immune response and inflammatory response, apoptosis inducing factors and enriched in JAK-STAT and MAPK signaling pathways. TXNIP (thioredoxin-interacting protein) gene was further demonstrated to play an important role participating in cellular apoptosis induced by EV71, and the apoptosis and death mediated by TXNIP during EV71 infection was triggered by viral 2A protease (2A^{pro}), not 3C protease (3C^{pro}).

Conclusion Our study demonstrated that RD cells have a significant response to EV71 infection, including immune response and apoptosis. 2A^{pro} might be a key inducer relative to the cellular apoptosis and death mediated by TXNIP during EV71 infection. These data would contribute to preferably understand the process at the molecular level and provide theoretical foundation for diagnosis and treatment of EV71-related diseases.

Keywords Enterovirus 71 (EV71) · RNA-Seq analysis · Apoptosis · TXNIP (thioredoxin-interacting protein) · 2A protease (2A^{pro})

Chenguang Yao and Kanghong Hu contributed equally.

Electronic supplementary material The online version of this article (<https://doi.org/10.1007/s13258-018-0760-7>) contains supplementary material, which is available to authorized users.

✉ Yanhong Wei
weiyanhong925@163.com

¹ National “111” Center for Cellular Regulation and Molecular Pharmaceutics, Hubei Key Laboratory of Industrial Microbiology, Key Laboratory of Fermentation Engineering (Ministry of Education), Hubei Provincial Cooperative Innovation Center of Industrial Fermentation, Sino-German Biomedical Center, Hubei University of Technology, 430068 Wuhan, China

Introduction

Enterovirus 71 (EV71) is a single positive-stranded RNA virus that belongs to the *Enterovirus* genus of the Picornaviridae family, which was first identified in 1969 in California (Schmidt et al. 1974). EV71 is the major causative agent of hand-foot-and-mouth disease (HFMD) and many neurological disorders, including encephalitis, acute flaccid paralysis, pulmonary edema (PE), or hemorrhage, culminating in fatality (Huang et al. 1999; Ho et al. 1999; Perez-Velez et al. 2007; Omana-Cepeda et al. 2016), and mainly affects infants and young children. Recent reports showed EV71 caused several large-scale outbreaks of severe complications (Mao et al. 2016; Sun et al. 2016). 126 deaths were caused by EV71 infection in China in 2008 (Yang et al. 2009; Chen et al. 2014) and the largest outbreak in China occurred in 2010, with an estimated 1.7 million infections; of which

27,000 were suffered with severe neurological complications, resulting in 905 fatalities (Zeng et al. 2012). Fatal cases were also reported in other countries in 2012 (Yang et al. 2009; Chen et al. 2014). EV71 infection has become a major public health threat across Asia Pacific.

However, there is no approved antiviral drug for EV71-induced disease because of high genomic mutation rates and lack of understanding of EV71 pathogenesis. Therefore, further investigation on the pathogenesis of EV71 infection has kindled considerable research interests in the field of medical virology. The susceptibility to establish infection directly correlates to the interaction between the hosts and pathogens. During infection, viruses modify host gene expression profiles to enhance their survival. Such activities include altering the cellular microenvironment to allow successful virus replication and evasion of the host immune system (Scaria et al. 2006; Ghosh et al. 2009; Roberts and Jopling 2010). Elucidating the underlying mechanisms that use to establish infections will provide a better understanding of the pathogenesis mechanism of the EV71 and thus aid in the development of potential antiviral therapeutics against EV71. Comparative analysis of genome-wide expression profiles are increasingly being applied to study virus-host interactions. The transcriptomic analysis of rhabdomyosarcoma (RD) cells infected with EV71 for 8 h or 20 h have proved a few genes, such as APOB and CLU (Leong and Chow 2006). Several EV71 proteins with unique functions have also been identified (Falk et al. 1990; Tesar and Marquardt 1990). However, a comprehensive understanding of the interaction between EV71 and the host RD cells is yet to be discovered.

EV71 infection is often accompanied by the apoptosis of host cells. Apoptosis, also called programmed cell death, is an important cell regulation mechanism in response to viral infections. Apoptosis possesses a complicated mechanism that involves a network of cross-talks and multiple specifically controlled pathways. EV71 infection can induce apoptosis in various cell types through different mechanisms (Chang et al. 2004). Understanding the molecular basis of the host response to microbial infection particularly anti-apoptotic responses, is essential for identifying targets to prevent EV71-induced diseases and tissue damages resulting from the inflammatory responses (Desagher and Martinou 2000).

TXNIP (thioredoxin-interacting protein), initially discovered as a vitamin D3-induced gene and an inhibitor of TRX (thioredoxin), mediates inhibition of cell proliferation and proapoptotic function through activation of apoptosis signal regulating kinase 1 (ASK1) (Chen et al. 2011). It could be a tumor suppressor gene (TSG) which is commonly silenced by genetic or epigenetic mechanisms in various cancers like hepatocellular carcinoma (HCC) (Kwon et al. 2010), breast cancer (Butler et al. 2002), bladder cancer (Nishizawa et al.

2011) and leukemia (Zhou et al. 2011). TXNIP was also demonstrated up-expressed in mRNAs and proteins during hepatitis B/C virus infection, which promoted host cell apoptosis (Blackham et al. 2010; He et al. 2017). However, its function in EV71-mediated apoptosis is still elusive.

In this study, RNA-Seq technology was used to assess the cell-specific transcriptional responses of cultured RD cells following infection with EV71. TXNIP gene, a critical molecule involving in cell apoptosis process, was screened and further studied from the RNA-seq analysis. Our study demonstrated that 2A^{PTO} might be a key inducer relative to the cellular apoptosis and death mediated by TXNIP during EV71 infection. These data would contribute to preferably understand the process at the molecular level and provide theoretical foundation for diagnosis and treatment of human EV71-related diseases.

Materials and methods

Manipulation of cells and viruses

RD cells were maintained in DMEM that contained 10% fetal bovine serum (FBS) (Gibco) at 37 °C with 5% CO₂ in a humidified incubator. Cells were split into a ratio of 1:4 in fresh medium every two days. After the RD cells had grown to 80% confluence, EV71 strain (GenBank accession no.KF501389.1) was inoculated into the cells at 37 °C for 1.5 h, and then the cells were further incubated in DMEM with 2% FBS at 37 °C, 5% CO₂.

Plasmids constructions

To generate pEGFP-2A, pEGFP-2A_{mut} (with Cys110 replaced by Ser), pEGFP-3C and pcDNA-TXNIP plasmids, the backbone plasmid pEGFP-C1 was digested with *Hind*III and *Bam*HI, and pcDNA3.1(+) was digested with *Hind*III and *Eco*RI. The cDNA fragments of EV71 genes were amplified from the total RNA extracts from RD cells infected with EV71 for 24 h, then were inserted into the appointed vectors. Primers : 2A forward, 5' AAGCTTATG GGGAAATTCGGTCAGCAGTC 3', reverse, 5' GGATCC TTAGCTCCATCGCTTCCTCA 3'; 2A_{mut} (the same terminal primers with 2A) forward, 5' TTCAGAACCTGG TGATTCTGG 3', reverse, 5' CCATCTAAGAATACCGCC AGA 3'; 3C forward, 5' AAGCTTTTATTGCTCGCTGGC AAAATAAC3', reverse, 5' GGATCCATGGGGCCCAGC TTAGACTTCG 3'; TXNIP forward, 5' GCCACCAAGCTT ATGGTGATGTTCAAGAAGATCAAGT 3', reverse, 5'CCG AATTCTCACTGCACATTGTTGTTGAGG 3'. All plasmids were expanded in DH5 α and purified with Endo-free Plasmid Mini Kit II (OMIGA).

Cell transfection

RD cells were cultured in 12-well plate over night until the intensity reached ~80% confluency. 2 μ g plasmids and 2 μ L lipofectamin 2000 Reagent (Invitrogen) were mixed with 100 μ L of opti-MEM maintaining for 20 min and then dropwise added to each cultural wells containing 200 μ L of opti-MEM. Following cultivation for 5 h, supernatants were replaced with fresh medium with 2% FBS to keep cell growing regularly.

Cell viability detection

Cell viability was measured by the MTT [3-(4,5-dimethylthiazol-2-yl)-2,5-diphenyltetrazoliumbromide] colorimetric method. Briefly, RD cells were plated in 96-well cell culture plate and cultured until cells reached ~80% confluency, then treated with 100TCID50 EV71 or transfected with 0.3 μ g plasmids (pEGFP-2A, pEGFP-3C, pEGFP and pEGFP-2Amut). Culture medium was removed and cells were washed with PBS. 5 mg/mL MTT reagent was added for 4 h. 50 μ L DMSO was added to each well to solubilize the formazan. Subsequently, the absorbance at 490 nm was recorded using an automatic plate reader (Biotek, Elx800). The survival rate was determined using the following formula: cell viability (%) = $(OD_{490}$ of treated cells - OD_{490} of blank) / (OD_{490} of control cells - OD_{490} of blank). Data were analyzed by GraphPad Prism 5.0 software.

Total RNA preparation

Total cellular RNA was extracted from uninfected, infected or transfected RD cells for RNA-Seq or qRT-PCR. Upon the completion of incubation, the culture supernatant was removed and cells were washed three times in sterile PBS. Total RNA was prepared from uninfected, infected or transfected RD cells with RNAiso Plus (Takara Bio Inc) in the dish (1 mL RNAiso per 10 cm²). Finally the RNA was suspended in nuclease-free water, and quantified by UV spectrophotometer at 260 nm. The integrity of the extracted RNA was confirmed by electrophoresis on a 1% denaturing agarose gel.

RNA-Seq analysis

RNA-Seq analysis was performed by BGI Tech company (Shenzhen, China) (Chen et al. 2015). Briefly, after the total RNA extraction and DNase I treatment, the mRNA was isolated using magnetic oligo (dT) beads and chopped into short fragments. Then cDNA were synthesized using the mRNA fragments as templates. The suitable fragments purified by agarose gel electrophoresis were selected for the PCR amplification as templates. During the QC (Quality

control) steps, Agilent 2100 Bioanalyzer and ABI StepOnePlus Real-Time PCR System were used in quantification and qualification of the sample library. Finally, the library was sequenced using Illumina HiSeq 2000.

Primary sequencing data that produced by Illumina HiSeq 2000, were called as raw reads. To decrease data noise, all the raw data were filtered by removing the reads with adapts, unknown bases and low quality to get “clean reads” for downstream bioinformatics analysis. Clean reads were mapped to reference sequences using SOAPaligner/SOAP2. The gene expression levels were evaluated by a software package RSEM (RNASeq by Expectation Maximization), and p values were calculated according to the poisson distribution. The threshold $p < 0.05$ and the fold change ($\log_2^{\text{ratio}} > 1$) were set to judge the significance of gene expression difference. To further process analysis, DAVID online tool (<http://david.abcc.ncifcrf.gov>) were used further to perform Gene Ontology (GO) enrichment analysis and KEGG pathway enrichment analysis (Huang et al. 2007, 2009).

Annexin-V-FITC/PI staining and flow cytometry

RD cells cultured in 12-well plate were transfected with control plasmids like pEGFP-C1, pEGFP-2Amut and pcDNA3.1(+) or over-expressing plasmids like pEGFP-3C, pEGFP-2A and pcDNA-TXNIP with lipofectamin 2000. Following incubation for 24 h or 48 h, cells were washed twice with cold 1 \times PBS (pH 7.4), and then cell apoptosis assay was performed using Annexin V-FITC/PI apoptosis detection kit [MultiSciences (LiankeBio)] following the manufacture’s protocol. Cell apoptosis level was measured by flow cytometry (BD Accui C6, BD Biosciences, USA) and analyzed by FlowJo software (USA).

qRT-PCR assay

After seeded in 24-well plate overnight, RD cells were infected with EV71 or transfected with control plasmids like pEGFP-C1, pEGFP-2Amut and pcDNA3.1(+) or over-expressing plasmids like pEGFP-3C, pEGFP-2A and pcDNA-TXNIP. Total intracellular RNA was extracted using a RNAiso Plus (Takara Bio Inc) Reagent. The RNA samples were detected using a real-time reverse-transcriptase polymerase chain reaction (RT-PCR) instrument (LightCycler 96, Roche) in accordance with the manufacturer’s instructions. A quantitative RT-PCR assay was performed using a PrimeScript RT reagent kit and SYBR Premix Ex Taq II (TaKaRa) following the manufacturer’s protocol. All the primers (Table 1) were designed using software primer 5.0. β -actin gene was used as the reference gene.

Table 1 The list of primers for qRT-PCR

Genes	Primers (For.)	Primers (Rev.)
TXNIP	F: TGGTGATCATGAGACCTGGA	R: AGGGGTATTGACATCCACCA
ZNF177	F: CTAGCCCATGCAAAGTAGG	R: GCAGCACAGGATTAGTGCAA
FUT1	F: TGGAAAAGCTGGGGTAGTTG	R: TGGATCCCTGGAAAGTTCTG
CCDC180	F: CTGGGAGAGCAGTGAGAACC	R: GCCTGGCTCTGATACTCCAG
GOLGAL	F: GCATTCCAGCAGGAGCTAAC	R: TTATTGCCGAGCTTGAATCC
RGPD1	F: CGTCCTGTTCAACACACCAA	R: CCTGTGGTCTGAGGGTGTCT
MEF2B	F: GACCGTGTGCTGCTGAAGTA	R: AGCCTCCGAAACTTCTCTCC
SERF1A	F: ATGGCCCGTGGAAATCAAC	R: TCTGAGAGGCAGTCAAGCTATC
RICTOR	F: ACTGCTTGCCAACCCTAATG	R: TGGTGTGTTGCAATTGCTTT
SPATAO	F: CAGACGACCTCCTCCTGAAG	R: CACCTCACCCAGGATCTCAC
CBWD6	F: TAGAAACGGTTGCCTCTGCT	R: TCACTCCCTAATTCGGCATC
NBPF11	F: TGTTTAGACCCAGGCAAAGG	R: CTCGGAGAGTCCACCAGAAG
HIST1H4K	F: TACTGCGCGACAATATCCAG	R: CAACCACCGAAACCGTAGAG
KLRK1	F: TTTTCAACACGATGGCAAAA	R: TCGGTCAAGGGAATTTGAAC
RN7SL2	F: CCAGGAGTTCTGGGCTGTAG	R: ATCAGCACGGGAGTTTTGAC
β -actin	F: ACCGCGAGAAGATGACCCAG	R: CCATCTCGTTCTCGAAGTCCA
VP1	F: GCAGCCCAAAAGAACTTCAC	R: ATTCAGCAGCTTGGAGTGC

Western blotting

Western blotting analyses were performed to examine intracellular protein levels of RD cells uninfected, infected with EV71 or transfected with plasmids. 20 μ g of total protein was separated on SDS-PAGE gels and then transferred to PVDF membranes. The membranes were blocked with 5% (w/v) nonfat milk in TBS tween buffer (TBST, 0.1%, v/v) for 1 h and then incubated with primary antibodies either TXNIP (dilution 1:2000) or β -actin (dilution 1:1000) at 4 °C overnight or at room temperature (RT) for 2–3 h. All the primary antibodies were purchased from Abcam (UK). After three washes in TBST, the membranes were incubated with secondary HRP-antibodies at RT for 1 h and washed again. Chemiluminescence detection was performed by ECL (Pierce, Rockford, USA).

Immunofluorescence microscopy

This method was conducted as described previously. (Yao et al. 2018) The EV71 VP1 monoclonal antibody and the Alexa-Fluor-488-labeled secondary antibody were purchased from ABcom company.

Statistical analysis

Data are presented as mean \pm SD of three independent experiments performed in triplicate. A t-test was used to compare groups, and $p < 0.05$ was considered statistically significant, unless otherwise specified. In Gene Ontology and DAVID analysis, the statistical data were generated by the software itself.

Results

Growth kinetics of EV71-infected RD cells

In order to determine the cellular growth kinetics and the cellular morphology post infection (p.i.) with EV71, four gradient viral titers (10TCID₅₀, 100TCID₅₀, 1000TCID₅₀, 10000TCID₅₀) and four gradient time points (12 h, 24 h, 32 h and 48 h p.i.) were set to make a microscopic examination. Increasing the viral titer could improve the base of EV71 replication, resulting in reduction of survival time (Fig. 1a). 100TCID₅₀ of EV71 was used in the following infection test. Compared to mock-infected control, no morphological difference was observed at 12 h, and 24 h p.i. However, at 32 h p.i., visible cytopathic effect (CPE) was observed and EV71 infection induced a significant CPE including rounding up, aggregation, and death, at 48 h p.i. (Fig. 1b), which was consistent with the analysis of cell viability (Fig. 1c). Besides, the viral RNA and protein levels were gradually increased in RD cells over time during persistent infection with EV71 (Fig. 1d, e). Although high levels of viral RNAs and proteins were detected in cells at 24 h p.i., no visible CPE was observed.

Transcriptome sequencing and differentially expressed genes (DEGs) analysis

To better elucidate the response of RD cells against EV71 infection at molecular level, RNA-Seq technology was used to determine the gene expression spectrum of RD cells infected or uninfected with EV71 for 24 h. After incubation, the samples were harvested and subjected

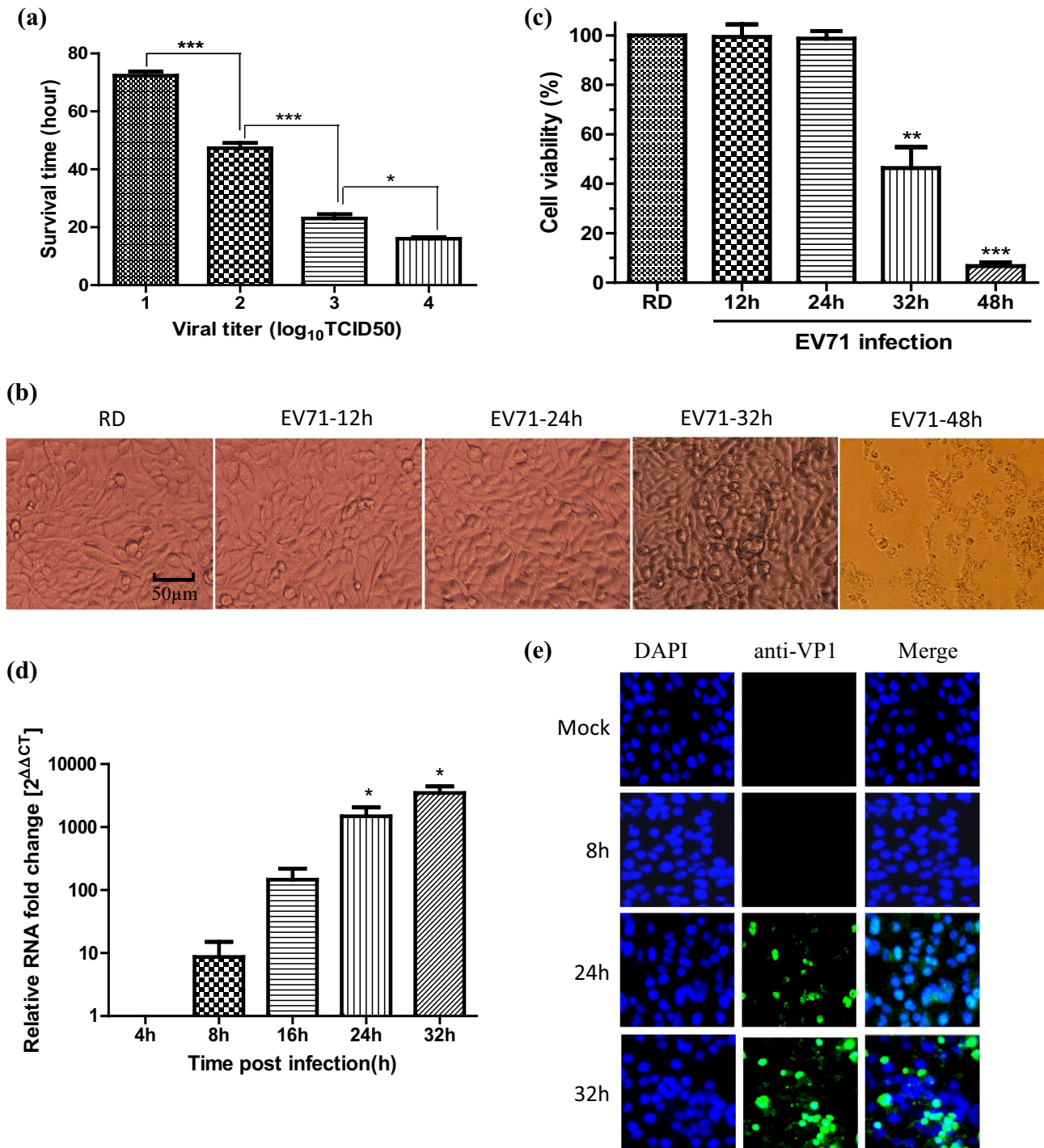


Fig. 1 The growth kinetics of EV71-infected RD cells. **a** The cell survival time related to different viral titers was determined by microscope observation. The cell survival time is defined as the time from virus inoculation to more than 75% of deaths. RD cells infected with 100 TCID₅₀ of EV71 were incubated for the indicated times p.i. **b** The cellular morphology was observed and captured by microscope (magnification, $\times 20$). **c** The cell viability was determined using MTT assay. ** $p < 0.01$, *** $p < 0.001$, compared with cell control. **d** Total

RNA was extracted from cells and EV71 RNA levels were measured. The data of 4 h was compared with that of other time points. Values represent the means \pm SDs of three independent experiments. * $p < 0.05$, compared with the RNA level at 4 h p.i. **e** Immunofluorescence microscopy of uninfected and EV71-infected RD cells at 8, 24 and 32 h p.i. Infected cells were detected by anti-VP1 (a structural protein of EV71) monoclonal antibody, while the cell nuclei were displayed by DAPI staining

to library construction and sequencing. In this analysis, more than 29 million reads for each sample were generated from constructed RNA-seq library using the Illumina HiSeq 2000 platform, in which the perfect match for each sample occupied about 50 percent (Table 2).

The total number of genes detected in each subject exceeded 15,000, and the majority of which were co-expressed (Fig. 2a). Among them, 329 differentially expressed genes (DEGs) were identified ($p < 0.05$, fold change (\log_2^{ratio}) > 1 or greater) between RD cells infected with EV71 and uninfected cells by clustering analysis

(Fig. 2b), 199 genes were up-regulated and 130 genes were down-regulated (Table S1).

Gene ontology (GO) and pathway enrichment analysis of differentially expressed genes (DEGs)

To determine the major biological themes in this data set, the Gene Ontology (GO) enrichment analysis and KEGG pathway enrichment analysis were performed using DAVID Bioinformatics Resources 6.8 (<https://david.ncifcrf.gov/>). GO molecular functional enrichment results showed that the DEGs were mainly related to metal ion binding, DNA

Table 2 Statistics of RNA-seq data and mapped reads obtained by an RNA-Seq analysis of RD cells infected or uninfected with EV71

Map to gene	Uninfected sample		EV71-infected sample	
	Reads number	Percent (%)	Reads number	Percent (%)
Total reads	30116036	100.00	29743214	100.00
Total mapped reads	21556212	71.58	18911124	63.58
Perfect match	14012109	46.53	12875813	43.29
mismatch	7544103	25.05	6035311	20.29
Unique match	16212202	53.83	15150180	50.94
Multi-position match	5344010	17.74	3760944	12.64
Total unmapped reads	8559822	28.42	10832088	36.42

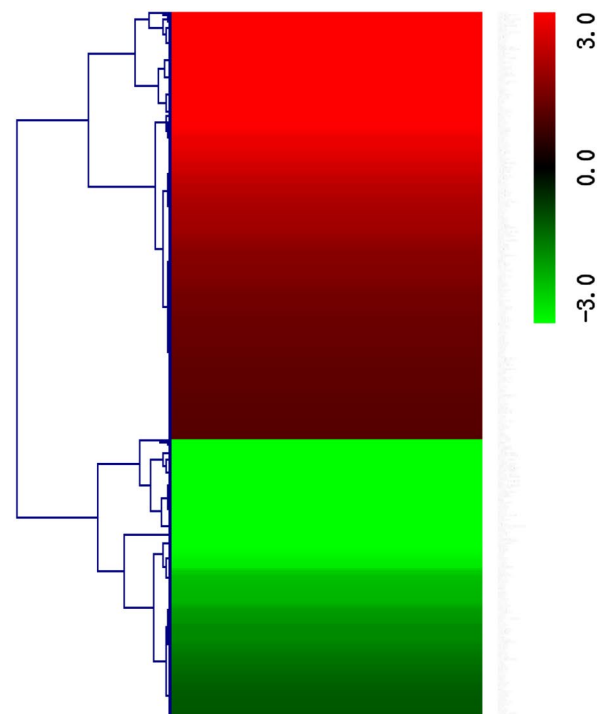
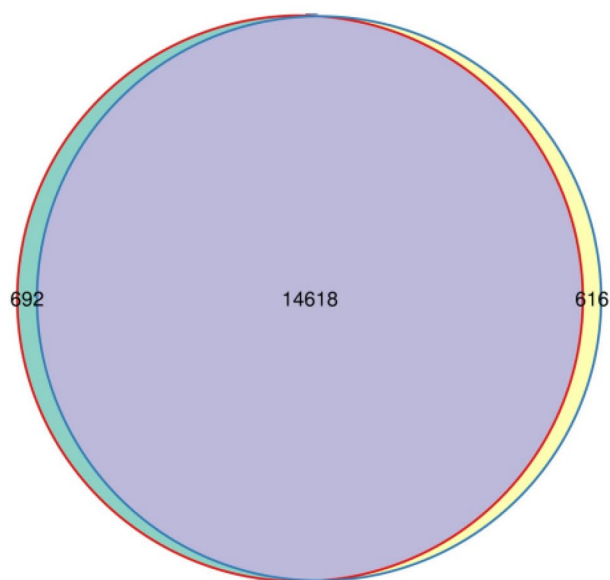


Fig. 2 Overview of the gene expression in RD cells infected or uninfected with EV71. **a** The Venn diagram shows the total number of overlapping genes for both samples (RD cells infected or uninfected with EV71). The red cycle represents the genes from uninfected sample, and the blue cycle represents the genes from EV71-infected

sample. **b** The heat maps of gene expressions. Red colour labels up-regulated genes and green colour labels down-regulated genes. The fold-change in gene expression was transformed to \log_2^{Ratio} . (Colour figure online)

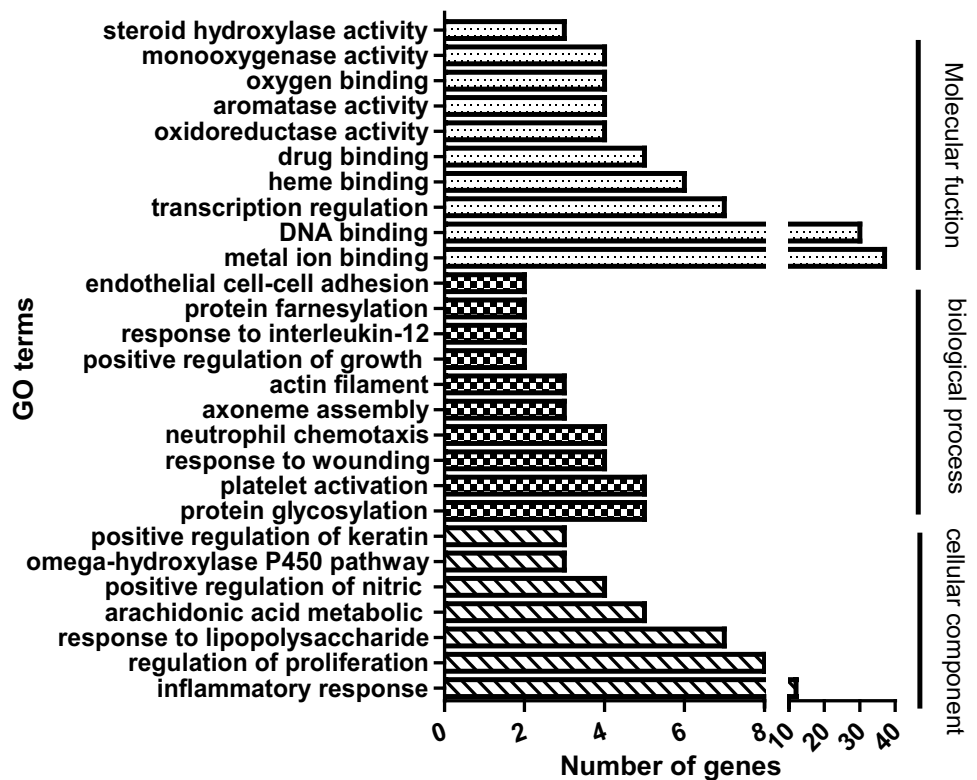
binding and transcription regulation (Fig. 3 and Table S1). There were 22 up-regulated genes enriched in metal ion binding and 18 up-regulated genes enriched in DNA binding, (Table S2). 7 down-regulated genes were enriched in protein heterodimerization activity (Table S3). We also annotated the DEGs into biological process, and the results illustrated that the up-regulated genes were aggregated in protein glycosylation, ion transport, nervous system development and positive regulation of cell proliferation (Table S2), while the down-regulated genes were mainly involved in negative regulation of cell proliferation, arachidonic acid metabolic process, platelet activation and angiogenesis (Table S3). Furthermore, GO cellular component analysis found some hub genes enriched in inflammatory response, lipopolysaccharide, integral component of plasma membrane, etc. (Fig. 3).

To explore the interaction between EV71 and RD cells, some typical DEGs were filtered according to its significance and GO enrichment score. Generally, viruses changed the host RNA network through disturbing its genetic smooth, which may therefore play a fundamental role in the regulation of viral replication, infection establishment, and viral pathogenesis (Li et al. 2014). 12 up-regulated genes and 6 down-regulated genes in Zinc finger protein family were identified, which involved in DNA binding and transcriptional regulation. It was reported that the 3C protease of EV71 could counteract the activity of host zinc-finger antiviral protein (ZAP) (Xie et al. 2018), which was also

verified in our present study. Cytochrome P450 family member CYP1B1 (fold change (\log_2^{ratio}) = -2.21, $p = 0.040$), CYP2U1 (fold change (\log_2^{ratio}) = -2.15, $p = 0.040$), CYP2D6 (fold change (\log_2^{ratio}) = -3.22, $p = 0.007$) and CYP1A1 [fold change (\log_2^{ratio}) = 1.05, $p = 0.048$] expressed at lower levels, which might be related to electron transfer in the inner membrane of mitochondria or in the endoplasmic reticulum (Berka et al. 2011). Previous studies had verified that coxsackievirus B3 (CVB3), also belongs to the *Enterovirus* genus, suppressed the expression of CYP-gene (Lundgren et al. 2007). Here, we confirmed that EV71 infection affected CYP-gene expression differently. As the core components of nucleosome, histone cluster family members HIST1H4K (fold change (\log_2^{ratio}) = -13.05, $p = 0.004$), HIST2H2AB (fold change (\log_2^{ratio}) = -11.64, $p = 0.046$) and HIST1H2AE (fold change (\log_2^{ratio}) = -3.30, $p = 0.007$) expressed lower markedly, while HIST1H4J emerged wide difference (fold change (\log_2^{ratio}) = 13.17, $p = 0.001$) (Table S1). It meant that histone cluster family members might be regulated greatly during EV71 infection. Moreover, it was reported that TXNIP (Thioredoxin-interacting protein) gene increasingly expression elevated the production of reactive oxygen species (ROS), and oxidative stress, resulting in cellular apoptosis (Zhou and Chng 2013). TXNIP gene was detected up-regulated expression (fold change (\log_2^{ratio}) = 1.52, $p = 5.02E-27$) in this study.

KEGG pathway enrichment analysis showed that DEGs were mainly enriched for terms related to malaria, ovarian

Fig. 3 GO enrichment analysis of differential expressed genes. GO enrichment analysis was provided by DAVID Bioinformatics Resources 6.8 (<https://david.ncifcrf.gov/>). The differential expressed genes were determined with $p < 0.05$ and fold change (\log_2^{ratio}) > 1 or greater. Molecular function, biological process and cellular components were enriched with $p < 0.05$ and gene number > 2 or more



steroidogenesis and leishmaniasis, most of which encoded transforming growth factors, transcription factors, janus kinase, cytochrome, cell adhesion molecules and apoptosis inducing factors (Table 3). Here, we found these genes were differentially regulated during EV71 infection. Taken together, these results suggested that RD cells have a significant response to EV71 infection, including immune response and apoptosis.

qRT-PCR analysis confirmed modified transcription of genes of interest during EV71 infection

In order to validate the results from RNA-Seq analysis, according to molecular functional classification, fourteen DEGs, including eight up-regulated genes and five down-regulated genes, were selected for further validation by qRT-PCR. These genes were of significant fold changes and mainly involved in immune response and apoptosis. House-keeping gene β -actin was used as a reference. The relative fold change was calculated based on an endogenous control for normalization and repeated three times independently. As shown in Table 4, relative to uninfected cells, most gene expression revealed consistent trends with transcriptome sequencing, including TXNIP, ZNF177, FUT1, CCDC180, GOLGAL, RGPDI, SERF1A, HIST1H4K, CBWD6,

NBPF1 and RN7SL2, while SPATAO showed weak down-regulation. To explore the interaction between RD cells and EV71, TXNIP gene with significant differential expression was selected for further study.

TXNIP up-regulation induced cellular apoptosis during EV71 infection

It is known that thioredoxin binding protein (TXNIP) has multiple functions and plays an important role in redox homeostasis, which increases the production of reactive oxygen species (ROS), and oxidative stress, resulting in cellular apoptosis (Zhou and Chng 2013; Yoshihara et al. 2014). Both RNA-Seq and qRT-PCR analysis demonstrated that TXNIP mRNA expression increased in RD cells infected with EV71. Western blot technique was also used to detect its protein expression levels at different time points. The results showed that the up-regulated TXNIP gene expression induced by EV71 infection revealed time independence within 36 h (Fig. 4a). To verify whether TXNIP over-expression can lead to RD cells apoptosis or death, pcDNA3.1 (also simply called pcDNA in this study) and pcDNA-TXNIP plasmids were transfected into RD cells. Annexin-V-FITC/PI stain and flow cytometry were used to detect cell apoptosis. TXNIP mRNA levels increased dramatically following pcDNA-TXNIP transfection compared to

Table 3 List of DEGs enriched in KEGG pathway

Pathway map	KEGG pathway	p value	Differential expressed genes enriched
hsa05144	Malaria	0.0141	TGFB2 THBS4 KLRK1 ITGB2
hsa04913	Ovarian steroidogenesis	0.0141	JMJD7-PLA2G4B PLA2G4B CYP1A1 CYP1B1
hsa05140	Leishmaniasis	0.0374	TGFB2 ITGB2 FOS JAK2

Table 4 Validation of differentially expressed genes by qRT-PCR

Genes	Fold change (\log_2^{ratio})		Up and down	Gene discription
	Transcriptome sequencing	qRT-PCR		
TXNIP	1.34	1.52	Up	Thioredoxin interacting protein
ZNF177	10.14	1.47	Up	ZNF559-ZNF177 readthrough
FUT1	8.27	1.33	Up	Fucosyltransferase 1 (galactoside 2-alpha-L-fucosyltransferase, H blood group)
CCDC180	9.17	0.52	Up	Coiled-coil domain containing 180
GOLGAL	9.51	0.50	Up	Golgin A8 family, member T
RGPDI	8.17	0.45	Up	RANBP2-like and GRIP domain containing 1
MEF2B	-10.37	0.32	Up	Myocyte enhancer factor 2B
SERF1A	12.40	0.21	Up	Small EDRK-rich factor 1A (telomeric)
SPATAO	1.05	-0.09	Down	Spermatogenesis associated 32
HIST1H4K	-13.05	-0.62	Down	Histone cluster 1, H4k
CBWD6	-11.77	-0.48	Down	COBW domain containing 6
NBPF1	-2.08	-0.44	Down	Neuroblastoma breakpoint family, member 1
RN7SL2	-1.97	-1.82	Down	RNA, 7SL, cytoplasmic 2

that of the control cells for both 24 h and 48 h (Fig. 4b). Furthermore, western blotting assay also displayed that TXNIP protein levels were prominent in the pcDNA-TXNIP transfected cells (Fig. 4c), suggesting the stability of over-expressed TXNIP on both mRNA and protein levels. Moreover, early apoptosis of RD cells were detected post transfection with pcDNA-TXNIP, but control plasmid pcDNA did not induce any apoptosis (Fig. 4d). So it could be concluded that EV71 infection up-regulated TXNIP expression, thereby inducing cellular apoptosis.

EV71 2A^{pro} up-regulates TXNIP expression and induces cellular apoptosis and death

EV71 2A protease (2A^{pro}) and 3C protease (3C^{pro}) play important roles in interaction between virus and host cells. Protease 2A, which cleaves eIF4GI, results in a decrease in cap-dependent translation disturbing the expression of host genes regularly (Thompson and Sarnow 2003). Kuo et al., found that 2A^{pro} from EV71 exhibits an apoptosis-inducing effect as those from other EV and Human rhinovirus (HRV) (Kuo et al. 2002). EV71 3C protease cleavage inactivates CstF-64 and impairs the host cell polyadenylation in vitro, as well as in virus-infected cells (Weng et al. 2009). In this study, to investigate whether the cellular apoptosis and death induced by EV71 infection is triggered by EV71 functional protein 2A^{pro} or 3C^{pro}, pEGFP-2A and pEGFP-3C plasmids were transfected into RD cells to detect the cellular apoptosis and death state. As shown in Fig. 5a, 2A^{pro} and 3C^{pro} expressed in RD cells accompanied by the green fluorescent protein (GFP). Subsequently, obvious CPE was observed and inhibitory effects on the proliferation of RD cells were detected by a MTT assay following pEGFP-2A transfection for 24 h and 48 h, while pEGFP-3C transfection did not exert any significant inhibitory effects on the cell viability (Fig. 5b).

Furthermore, TXNIP mRNA was evaluated by qRT-PCR, and TXNIP protein was determined by western blotting analysis when pEGFP-2A plasmid was transfected into RD cells for 24 h and 48 h. As shown in Fig. 5c, d, the expression of TXNIP was tremendously induced at mRNA and protein levels in the pcDNA-2A transfected cells, while no obvious change was observed in the cells transfected with pcDNA-3C. Hence, 2A^{pro} might be a key inducer relative to the cellular apoptosis and death mediated by TXNIP during EV71 infection.

Discussion

There is currently no effective treatment for EV71 infection due to the lack of understanding of viral replication and infection. Thus, it is extremely critical to understand the

underlying mechanism of EV71 replication during its infection in order to prevent and control human EV71-related diseases. In order to uncover the pathological features of EV71 infection and host cellular responses, RNA-seq technology was performed to analysis the DEGs in RD cells. Because of visible CPE and high infectious titer in the later stage of EV71 infection (following 48 h infection with EV71 in this study), samples infected with EV71 for 24 h, were sequenced using Illumina HiSeq 2000 and validated by real-time RT-PCR. Antiviral transcriptional responses and regulations of cell death are crucial events of the host response to virus infection, thus these two aspects are focused on in this study.

Human whole genome microarray has been employed to monitor changes in genomic profiles between EV71 infected and uninfected cells. Leong et al., conducted host gene expression analysis in EV71-infected RD cells using microarray analysis (Leong and Chow 2006), which showed altered transcripts including those encoding components of cytoskeleton, protein translation and modification, cellular transport proteins, protein degradation mediators, cell death mediators, mitochondrial-related and metabolism proteins, cellular receptors and signal transducers. Human glioblastoma SF268 cells and SH-SY5Y cells were also used to study changes in mRNA expression during EV71 infection (Shih et al. 2004; Xu et al. 2013). These studies indicated that the host response varied significantly depending on the types of both host cells and viral strains. In this study, we utilized transcriptional sequencing to profile the kinetics and patterns of host gene expression in EV71 (EV71/wuhan/3018/2010)-infected RD cells. Generally, researchers pay more attention to the studies of international standard strains such as MS/7423/87 and BrCr strains of EV71, and ignore the studies of regional EV71 strain. However, genetic diversity including mutations and recombinants as well as the heterogeneity of antigenic properties among EV71 strains in different regional outbreaks are obvious. It is likely that there is a discrepancy between the major subgenogroups circulating in the Asia-Pacific region and those in Europe (Mizuta et al. 2014). It is necessary to analyze the host response to different EV71 strains in different regions, to develop reasonable strategies against severe EV71 infections. Hubei province of China has been an area with high incidence of EV71-related HFMD. In April 2011, an unpredicted HFMD outbreak in Xiangyang city of Hubei province resulted in a high aggregation of HFMD cases including fatal cases and many severe cases (Huang et al. 2018). Wuhan, capital city of Hubei province, with 10 million population, has also been threatend by serious EV71-related HFMD epidemic and has over 10,000 HFMD cases reported each year. Totally, 80,219 patients of 0–5 years experienced HFMD in 2010–2015 in Wuhan (Chen et al. 2017). EV71 strain (EV71/wuhan/3018/2010) in this study was isolated in Wuhan in 2010. The nucleotide

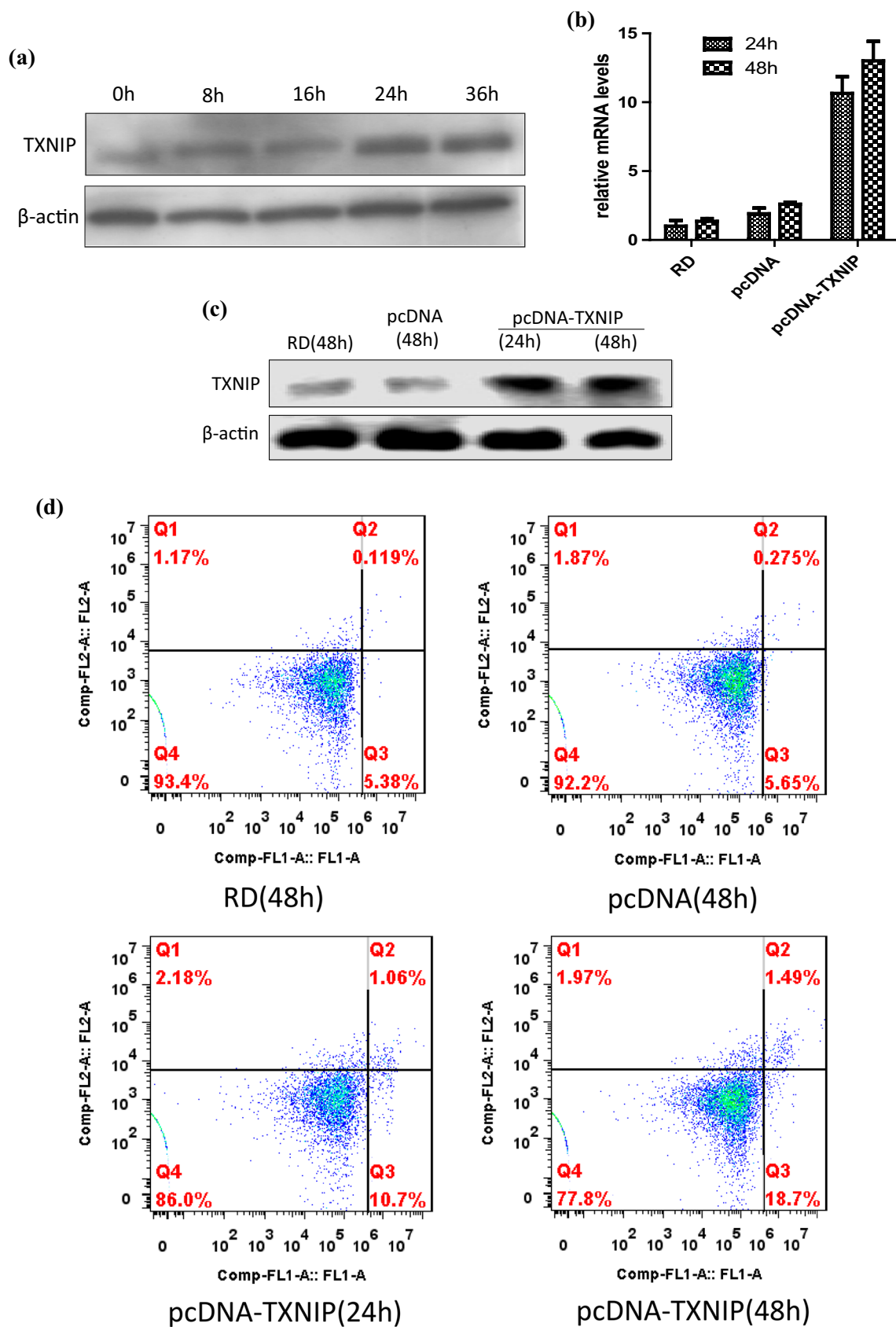


Fig. 4 TXNIP up-regulation induced cellular apoptosis during EV71 infection. **a** Western blot analysis of TXNIP expression at 0, 8, 16, 24 and 36 h p.i. Total protein extracts (20 µg/lane) were tested against the relevant specific antibodies. The β-actin housekeeping protein was used as a standard for equal loading of protein. **b** The indicated mRNAs levels of TXNIP were determined from cells transfected with (or without) pcDNA-TXNIP or control pcDNA by qRT-PCR. **c** Western blotting analysis of TXNIP protein expression following pcDNA-TXNIP or pcDNA control transfection. **d** RD cells were stained with annexin-V-FITC/PI after transfection with (or without) pcDNA or pcDNA-TXNIP for 24 h or 48 h, and cell apoptosis was determined by flow cytometry. All experiments were performed three times independently and the representative results were shown

sequences homology between EV71/wuhan/3018/2010 (KF501389.1) and EV71-Hubei-09-China (GU434 678.1), BrCr-TR (AB204852.1), BrCr-ts (AB204853.1) and BrCr-CA-70 strains were achieved 99% (Yang et al. 2013), which indicates that our study may contribute to a better understanding of the pathogenesis mechanism of EV71 strains and help to develop an appropriate therapeutic strategy in local area and provide a reference for the study of these related EV71 strains.

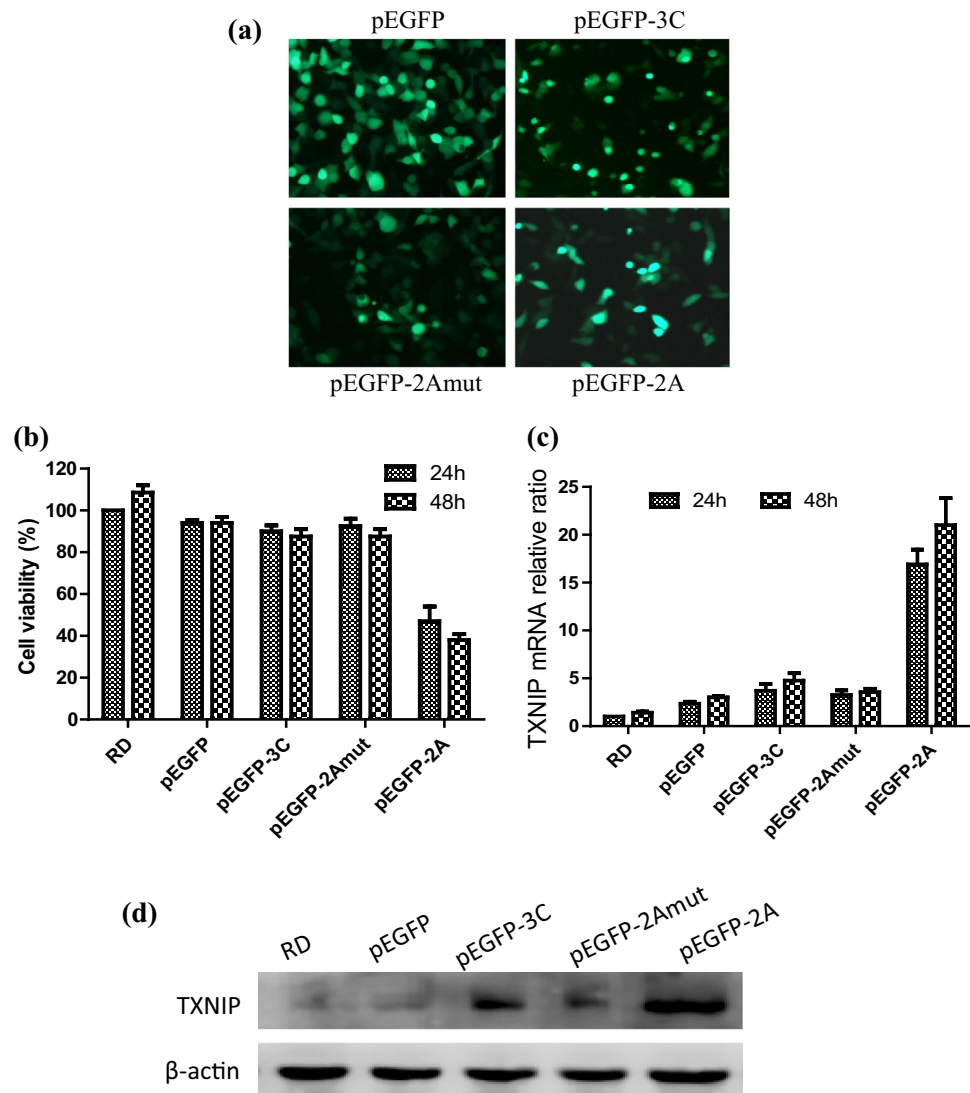
In our transcriptome data, 320 DEGs were filtrated to perform GO and KEGG pathway enrichment. The total DEGs were enriched in cellular component, biological process and molecular function (Fig. 3 and Table S1). Biological process results showed some genes were related to inflammatory response (12 genes), regulation of cell proliferation (19 genes), response to lipopolysaccharide (7 genes) and visual perception (6 genes). The inflammatory response genes included CXCL3, FOS, AGER, TNFRSF14, NFKBIZ, TMED7-TICAM2, LY75 and PLA2G4B up-regulation (Table S2). These responses revealed the host antiviral action against viral replication in the early stage. Meanwhile, another classical genes involved in regulation of cell proliferation were enriched, 8 up-regulated (Table S2) and 6 down-regulated (Table S3) genes were related to positive and negative regulation of cell proliferation. These responses in cellular proliferation during EV71 infection had been proved previously (Leong and Chow 2006).

GO functional classification analysis showed main DEGs classes including zinc finger protein family, zytochrome P450 family, and histone cluster family etc. 12 up-regulated genes and 6 down-regulated genes in zinc finger protein family were identified, which involved in DNA binding and transcriptional regulation. There were many reports on the close relationship between members of the zinc finger protein family and viral infections (Lukic et al. 2014; Shao et al. 2018). The zinc-finger protein (Z) serves as a main component required for virus budding from the membrane of the infected cells through self-oligomerization and it has also been shown to be essential for mediating viral transcriptional repression activity, thus limiting viral replication (Lukic et al. 2014; Shao et al. 2018). Moreover, ZNF136, a

cellular host factor, was identified to have interaction with truncated nonstructural protein 2 of hepatitis C virus (Liu and Chen 2014). However, more evidences need to be collected to clarify how the zinc finger family members work in host cells to struggle against EV71 infection. P450 (CYP) enzymes play a critical role in the metabolism of drugs and other xenobiotics. Antiretroviral drug (ARV) metabolism is linked largely to hepatic cytochrome P450 (CYP) activity (McMillan et al. 2018). Some drugs have been designed targeting to CYPs on HCV and HIV treatment in recent years (Ande et al. 2013; Midde and Kumar 2015; Sabo et al. 2015). In this study, the differential expressions of some CYPs were observed associated with EV71 infection, which might be of great significance for the design and development of antivirals against EV71 infection. Interestingly, the histone family members HIST1H2AE, HIST1H2AB, HIST1H4K and HIST1H4J showed significant changes on transcriptional level (Table S1). The foot-and-mouth disease virus (FMDV) 3C^{pro} including EV71 3C^{pro} catalyze the histone H3 transition and cleave at N-terminal (Falk et al. 1990; Tesar and Marquardt 1990). However, the relationship between EV71 and the other histone family members are not clear. Histone deacetylases (HDACs) that play a key role in the homeostasis of the acetylation level and inhibition of HDAC activity, were originally identified as a powerful anti-cancer therapeutic strategy and were recently found to be implicated in the regulation of the inflammatory response. Inhibition of HDAC activity elevates CVB3 viral replication (Zhou et al. 2015). So the variational expression of the histone cluster family members in RD cells infected with EV71 may contribute to EV71 replication. The down regulated gene with the maximum of fold change (\log_2^{ratio}) (-12.2 , $p=7.39E-35$) was INS-IGF2 (Table S1). INS-IGF2 gene includes two alternatively spliced read-through transcript variants which align to the INS gene in the 5' region and to the IGF2 gene in the 3' region. However, RNA sequencing fusion transcripts like INS were always mapped to INS-IGF2, so the signal of INS-IGF2 belonged to both INS-IGF2 and INS. EV71 may activate PI3K/AKT signaling pathway to trigger the anti-apoptotic effects at the early phase during infection (Autret et al. 2008), and INS-IGF2 serves as an initial activator in the PI3K/AKT pathway. In this analysis, the down-regulation of INS-IGF2 gene might inactivate PI3K/AKT pathway to induce apoptosis of cells.

KEGG pathway enrichment provided an explicable pathway called leishmaniasis, in which TGFB2, ITGB2, FOS and JAK2 were enriched ($p=0.0374$). TGFB signaling was significantly up-regulated in the advanced fibrosis stage of chronic hepatitis C (Chida et al. 2017), a significant positive correlation was observed between the expression of TGFB2 and decapentaplegic homolog 2 (Smad2), Smad2 and Foxo3a, and Foxo3a and Socs3 in the liver of chronic hepatitis C patients (Shirasaki et al. 2014). TGFB

Fig. 5 EV71 2A^{pro}, not 3C^{pro} up-regulated TXNIP expression inducing cellular apoptosis and death. **a** The expression of 2A^{pro} and 3C^{pro} accompanied by green fluorescent protein (GFP) were observed through fluorescent microscope when pEGFP-2A plasmid controlled with pEGFP-2Amut and pEGFP-3C plasmid controlled with pEGFP were transfected into RD cells for 24 h, respectively. **b** Cell viability was detected by MTT assay following transfection with plasmids presented in **a** for 24 h or 48 h. **c** TXNIP mRNA levels were measured by qRT-PCR following transfection of RD cells with plasmids presented in **a** for 24 h or 48 h. **d** TXNIP protein was determined by western blotting analysis. 20 µg samples, extracted from RD cells following transfection with plasmids presented in **a** for 24 h, were spotted in each lane. All experiments were performed three times independently and the representative results or the mean values, ±SD were shown



was also reported to involve in a novel inflammatory pathway mediated by macrophages leading to human retinal pericyte apoptosis (Betts-Obregon et al. 2016). However, there is no data on TGFB2 involving in EV71 infection. Activation of p42/p44 MAPK, p38 MAPK, JNK, PI3K/AKT and NF-kappaB related to FOS and JAK2 mediates EV71-induced response, which may be associated with the secretions of inflammatory cytokines and host cellular apoptosis (Shirasaki et al. 2014; Tung et al. 2010). NKG2D, also called KLRK1, is an activating receptor on T cells, which has been implicated in immunosuppressive effect and HBV infection (Dong et al. 2015). ITGB2 limits TLR signaling by inhibiting NF-κB pathway activation and promoting p38 MAPK activation, thereby fine-tuning TLR-induced inflammatory responses, even apoptosis (Choi et al. 2015). Moreover, JNK1/2 and p38 MAPK signaling pathways and phosphorylation of their downstream transcription factors c-Fos are beneficial to EV71

infection and positively regulate secretions of inflammatory cytokines (Zhang et al. 2014). EV71 infection also represses the JAK-STAT signaling pathway and interferon-stimulated gene expression (Peng et al. 2014).

TXNIP, a significantly up-regulated gene during EV71 infection, was put forward involving in cellular apoptosis and death for the first time. It was reported that Trx/Txnip, a redox-sensitive signaling complex, is a regulator of cellular redox status and a key component in the link between redox regulation and the pathogenesis of diseases (Blackham et al. 2010; Yoshihara et al. 2014). In this study, we illustrated TXNIP over-expression could lead to cellular apoptosis, and we also discovered EV71 infection up-regulated TXNIP expression and promoted cellular apoptosis. This study showed 2A^{pro} induced cellular apoptosis and death accompanied with TXNIP over-expression, while over-expression of 3C^{pro} was not obviously related to cellular apoptosis, which revealed the activation of TXNIP pathway

initiated by 2A^{pro} during EV71 infection could be a supplementary apoptosis inducer.

Taken together, our study provided important insights into dynamic transcriptome profile in finding EV71-host cell interactions and potential impact on understanding other enterovirus-host cell interactions. Further investigation on the activation of TXNIP dependent apoptosis pathway triggered by 2A^{pro} will contribute to understand the characteristics of EV71 pathogenesis, and may provide potential targets for clinical diagnosis and treatment of EV71-related HFMD.

Acknowledgements This work received financial support from the National Natural Science Foundation of China (31400153, to WYH), the Collaborative Grant-in-Aid of the HBUT National “111” Center for Cellular Regulation and Molecular Pharmaceutics (XBTK-2018005, to WYH), and the Doctoral Scientific Research Foundation of Hubei University of Technology (BSQD2015004, to WYH).

Author contributions Conceived the idea and initiated the work: WYH, YCG, & HKH. Contributed to design of experiments: WYH, HKH, YCG, & XCL. Performed the experiments: YCG, HKH, XCL & LN. Contributed reagents/materials/analysis tools: WYH, XCL, & LN. Analysis of experiments and results: WYH, YCG, & HKH. Contribution in generating graphics: YCG, & HKH. Writing of the manuscript: YCG & WYH. All the authors read and approved the manuscript.

Compliance with ethical standards

Conflict of interest All authors Chenguang Yao, Kanghong Hu, Caili Xi, Ni Li and Yanhong Wei declare that they have no conflict of interest.

Research involving human participants and/or animals This article does not contain any studies with human participants or animals performed by any of the authors.

References

- Ande A, McArthur C, Kumar A, Kumar S (2013) Tobacco smoking effect on HIV-1 pathogenesis: role of cytochrome P450 isozymes. *Expert Opin Drug Metab Toxicol* 9:1453–1464
- Autret A, Martin-Latil S, Brisac C, Mousson L, Colbere-Garapin F, Blondel B (2008) Early phosphatidylinositol 3-kinase/Akt pathway activation limits poliovirus-induced JNK-mediated cell death. *J Virol* 82:3796–3802
- Berka K, Hendrychova T, Anzenbacher P, Otyepka M (2011) Membrane position of ibuprofen agrees with suggested access path entrance to cytochrome P450 2C9 active site. *J Phys Chem A* 115:11248–11255
- Betts-Obregon BS, Mondragon AA, Mendiola AS, LeBaron RG, Asmis R, Zou T, Gonzalez-Fernandez F, Tsin AT (2016) TGFbeta induces BIGH3 expression and human retinal pericyte apoptosis: a novel pathway of diabetic retinopathy. *Eye (Lond)* 30:1639–1647
- Blackham S, Baillie A, Al-Hababi F, Remlinger K, You S, Hamatake R, McGarvey MJ (2010) Gene expression profiling indicates the roles of host oxidative stress, apoptosis, lipid metabolism, and intracellular transport genes in the replication of hepatitis C virus. *J Virol* 84:5404–5414
- Butler LM, Zhou X, Xu WS, Scher HI, Rifkind RA, Marks PA, Richon VM (2002) The histone deacetylase inhibitor SAHA arrests cancer cell growth, up-regulates thioredoxin-binding protein-2, and down-regulates thioredoxin. *Proc Natl Acad Sci USA* 99:11700–11705
- Chang SC, Lin JY, Lo LY, Li ML, Shih SR (2004) Diverse apoptotic pathways in enterovirus 71-infected cells. *J Neurovirol* 10:338–349
- Chen SC, Chang LY, Wang YW, Chen YC, Weng KF, Shih SR, Shih HM (2011) Sumoylation-promoted enterovirus 71 3C degradation correlates with a reduction in viral replication and cell apoptosis. *J Biol Chem* 286:31373–31384
- Chen JF, Zhang RS, Ou XH, Chen FM, Sun BC (2014) The role of enterovirus 71 and coxsackievirus A strains in a large outbreak of hand, foot, and mouth disease in 2012 in Changsha, China. *Int J Infect Dis* 28:17–25
- Chen F, Zhang C, Jia X, Wang S, Wang J, Chen Y, Zhao J, Tian S, Han X, Han L (2015) Transcriptome profiles of human lung epithelial cells A549 interacting with *Aspergillus fumigatus* by RNA-SEQ. *PLoS One* 10:e135720
- Chen Q, Xing XS, Wu Y, Liao QH, Liu GP, Jiang XQ, Guan XH (2017) Hand, foot and mouth disease in Hubei province, 2009–2015: an epidemiological and etiological study. *Zhonghua Liu Xing Bing Xue Za Zhi* 38:441–445
- Chida T, Ito M, Nakashima K, Kanegae Y, Aoshima T, Takabayashi S, Kawata K, Nakagawa Y, Yamamoto M, Shimano H, Matsuura T, Kobayashi Y, Suda T, Suzuki T (2017) Critical role of CREBH-mediated induction of TGF-beta2 by HCV infection in fibrogenic responses in hepatic stellate cells. *Hepatology* 66:1430–1443
- Choi MS, Jeong HJ, Kang TH, Shin HM, Oh ST, Choi Y, Jeon S (2015) Meso-dihydroguaiaretic acid induces apoptosis and inhibits cell migration via p38 activation and EGFR/Src/intergrin beta3 down-regulation in breast cancer cells. *Life Sci* 141:81–89
- Desagher S, Martinou JC (2000) Mitochondria as the central control point of apoptosis. *Trends Cell Biol* 10:369–377
- Dong S, Geng L, Shen MD, Zheng SS (2015) Natural Killer cell activating receptor NKG2D Is involved in the immunosuppressive effects of mycophenolate mofetil and hepatitis B virus infection. *Am J Med Sci* 349:432–437
- Falk MM, Grigera PR, Bergmann IE, Zibert A, Multhaup G, Beck E (1990) Foot-and-mouth disease virus protease 3C induces specific proteolytic cleavage of host cell histone H3. *J Virol* 64:748–756
- Ghosh Z, Mallick B, Chakrabarti J (2009) Cellular versus viral microRNAs in host-virus interaction. *Nucleic Acids Res* 37:1035–1048
- He Z, Yu Y, Nong Y, Du L, Liu C, Cao Y, Bai L, Tang H (2017) Hepatitis B virus X protein promotes hepatocellular carcinoma invasion and metastasis via upregulating thioredoxin interacting protein. *Oncol Lett* 14:1323–1332
- Ho M, Chen ER, Hsu KH, Twu SJ, Chen KT, Tsai SF, Wang JR, Shih SR (1999) An epidemic of enterovirus 71 infection in Taiwan. Taiwan Enterovirus Epidemic Working Group. *N Engl J Med* 341:929–935
- Huang CC, Liu CC, Chang YC, Chen CY, Wang ST, Yeh TF (1999) Neurologic complications in children with enterovirus 71 infection. *N Engl J Med* 341:936–942
- Huang DW, Sherman BT, Tan Q, Collins JR, Alvord WG, Roayaei J, Stephens R, Baseler MW, Lane HC, Lempicki RA (2007) The DAVID gene functional classification tool: a novel biological module-centric algorithm to functionally analyze large gene lists. *Genome Biol* 8:R183
- Huang DW, Sherman BT, Lempicki RA (2009) Systematic and integrative analysis of large gene lists using DAVID bioinformatics resources. *Nat Protoc* 4:44–57
- Huang J, Chen S, Wu Y, Tong Y, Wang L, Zhu M, Hu S, Guan X, Wei S (2018) Quantifying the influence of temperature on hand, foot and mouth disease incidence in Wuhan, Central China. *Sci Rep* 8:1934

- Kuo RL, Kung SH, Hsu YY, Liu WT (2002) Infection with enterovirus 71 or expression of its 2A protease induces apoptotic cell death. *J Gen Virol* 83:1367–1376
- Kwon HJ, Won YS, Suh HW, Jeon JH, Shao Y, Yoon SR, Chung JW, Kim TD, Kim HM, Nam KH, Yoon WK, Kim DG, Kim JH, Kim YS, Kim DY, Kim HC, Choi I (2010) Vitamin D3 upregulated protein 1 suppresses TNF- α -induced NF- κ B activation in hepatocarcinogenesis. *J Immunol* 185:3980–3989
- Leong WF, Chow VT (2006) Transcriptomic and proteomic analyses of rhabdomyosarcoma cells reveal differential cellular gene expression in response to enterovirus 71 infection. *Cell Microbiol* 8:565–580
- Li C, Hu J, Hao J, Zhao B, Wu B, Sun L, Peng S, Gao GF, Meng S (2014) Competitive virus and host RNAs: the interplay of a hidden virus and host interaction. *Protein Cell* 5:348–356
- Liu C, Chen X (2014) A potential cellular host factor homologous to ZNF-136 can interact with truncated nonstructural protein 2 of hepatitis C virus. *Arch Virol* 159:785–789
- Lukic S, Nicolas JC, Levine AJ (2014) The diversity of zinc-finger genes on human chromosome 19 provides an evolutionary mechanism for defense against inherited endogenous retroviruses. *Cell Death Differ* 21:381–387
- Lundgren M, Darnerud PO, Molin Y, Lilienthal H, Blomberg J, Ilback NG (2007) Coxsackievirus B3 infection and PBDE exposure causes organ-specific effects on CYP-gene expression in the mouse. *Toxicology* 242:91–99
- Mao QY, Wang Y, Bian L, Xu M, Liang Z (2016) EV71 vaccine, a new tool to control outbreaks of hand, foot and mouth disease (HFMD). *Expert Rev Vaccines* 15:599–606
- McMillan JM, Cobb DA, Lin Z, Banoub MG, Dagur RS, Branch WA, Wang W, Makarov E, Kocher T, Joshi PS, Quadros RM, Harms DW, Cohen SM, Gendelman HE, Gurumurthy CB, Gorantla S, Poluektova LY (2018) Antiretroviral drug metabolism in humanized PXR-CAR-CYP3A-NOG mice. *J Pharmacol Exp Ther* 365:272–280
- Midde NM, Kumar S (2015) Development of NanoART for HIV treatment: minding the cytochrome P450 (CYP) enzymes. *J Pers Nanomed* 1:24–32
- Mizuta K, Aoki Y, Matoba Y, Yahagi K, Itagaki T, Katsushima F, Katsushima Y, Ito S, Hongo S, Matsuzaki Y (2014) Molecular epidemiology of enterovirus 71 strains isolated from children in Yamagata, Japan, between 1990 and 2013. *J Med Microbiol* 63:1356–1362
- Nishizawa K, Nishiyama H, Matsui Y, Kobayashi T, Saito R, Kotani H, Masutani H, Oishi S, Toda Y, Fujii N, Yodoi J, Ogawa O (2011) Thioredoxin-interacting protein suppresses bladder carcinogenesis. *Carcinogenesis* 32:1459–1466
- Omana-Cepeda C, Martinez-Valverde A, Sabater-Recolons M, Jane-Salas E, Mari-Roig A, Lopez-Lopez J (2016) A literature review and case report of hand, foot and mouth disease in an immunocompetent adult. *BMC Res Notes* 9:165
- Peng H, Shi M, Zhang L, Li Y, Sun J, Zhang L, Wang X, Xu X, Zhang X, Mao Y, Ji Y, Jiang J, Shi W (2014) Activation of JNK1/2 and p38 MAPK signaling pathways promotes enterovirus 71 infection in immature dendritic cells. *BMC Microbiol* 14:147
- Perez-Velez CM, Anderson MS, Robinson CC, McFarland EJ, Nix WA, Pallansch MA, Oberste MS, Glode MP (2007) Outbreak of neurologic enterovirus type 71 disease: a diagnostic challenge. *Clin Infect Dis* 45:950–957
- Roberts AP, Jopling CL (2010) Targeting viral infection by microRNA inhibition. *Genome Biol* 11:201
- Sabo JP, Kort J, Ballow C, Kashuba AD, Haschke M, Battagay M, Girlich B, Ting N, Lang B, Zhang W, Cooper C, O'Brien D, Seibert E, Chan TS, Tweedie D, Li Y (2015) Interactions of the hepatitis C virus protease inhibitor faldaprevir with cytochrome P450 enzymes: in vitro and in vivo correlation. *J Clin Pharmacol* 55:467–477
- Scaria V, Hariharan M, Maiti S, Pillai B, Brahmachari SK (2006) Host-virus interaction: a new role for microRNAs. *Retrovirology* 3:68
- Schmidt NJ, Lennette EH, Ho HH (1974) An apparently new enterovirus isolated from patients with disease of the central nervous system. *J Infect Dis* 129:304–309
- Shao J, Liang Y, Ly H (2018) Roles of arenavirus Z protein in mediating virion budding, viral transcription-inhibition and interferon-beta suppression. *Methods Mol Biol* 1604:217–227
- Shih SR, Stollar V, Lin JY, Chang SC, Chen GW, Li ML (2004) Identification of genes involved in the host response to enterovirus 71 infection. *J Neurovirol* 10:293–304
- Shirasaki T, Honda M, Shimakami T, Murai K, Shiimoto T, Okada H, Takabatake R, Tokumaru A, Sakai Y, Yamashita T, Lemon SM, Murakami S, Kaneko S (2014) Impaired interferon signaling in chronic hepatitis C patients with advanced fibrosis via the transforming growth factor beta signaling pathway. *Hepatology* 60:1519–1530
- Sun J, Niu Y, Wang C, Zhang H, Xie B, Xu F, Jin H, Peng Y, Liang L, Xu P (2016) Discovery of 3-benzyl-1,3-benzoxazine-2,4-dione analogues as allosteric mitogen-activated kinase kinase (MEK) inhibitors and anti-enterovirus 71 (EV71) agents. *Bioorg Med Chem* 24:3472–3482
- Tesar M, Marquardt O (1990) Foot-and-mouth disease virus protease 3C inhibits cellular transcription and mediates cleavage of histone H3. *Virology* 174:364–374
- Thompson SR, Sarnow P (2003) Enterovirus 71 contains a type I IRES element that functions when eukaryotic initiation factor eIF4G is cleaved. *Virology* 315:259–266
- Tung WH, Hsieh HL, Yang CM (2010) Enterovirus 71 induces COX-2 expression via MAPKs, NF- κ B, and AP-1 in SK-N-SH cells: Role of PGE(2) in viral replication. *Cell Signal* 22:234–246
- Weng KF, Li ML, Hung CT, Shih SR (2009) Enterovirus 71 3C protease cleaves a novel target CstF-64 and inhibits cellular polyadenylation. *PLoS Pathog* 5:e1000593
- Xie L, Lu B, Zheng Z, Miao Y, Liu Y, Zhang Y, Zheng C, Ke X, Hu Q, Wang H (2018) The 3C protease of enterovirus A71 counteracts the activity of host zinc-finger antiviral protein (ZAP). *J Gen Virol* 99:73–85
- Xu LJ, Jiang T, Zhang FJ, Han JF, Liu J, Zhao H, Li XF, Liu RJ, Deng YQ, Wu XY, Zhu SY, Qin ED, Qin CF (2013) Global transcriptomic analysis of human neuroblastoma cells in response to enterovirus type 71 infection. *PLoS One* 8:e65948
- Yang F, Ren L, Xiong Z, Li J, Xiao Y, Zhao R, He Y, Bu G, Zhou S, Wang J, Qi J (2009) Enterovirus 71 outbreak in the People's Republic of China in 2008. *J Clin Microbiol* 47:2351–2352
- Yang Z, Lu S, Xian J, Ye J, Xiao L, Luo J, Zen K, Liu F (2013) Complete genome sequence of a human enterovirus 71 strain isolated in wuhan, china, in 2010. *Genome Announc* 1:e01112–13
- Yao CG, Xi CL, Hu KH, Gao W, Cai XF, Qin JL, Lv SY, Du CH, Wei YH (2018) Inhibition of enterovirus 71 replication and viral 3C protease by quercetin. *Virology J* 15:116
- Yoshihara E, Masaki S, Matsuo Y, Chen Z, Tian H, Yodoi J (2014) Thioredoxin/Txnip: redoxosome, as a redox switch for the pathogenesis of diseases. *Front Immunol* 4:514
- Zeng M, El KN, Tu S, Ren P, Xu S, Zhu Q, Mo X, Pu D, Wang X, Altmeyer R (2012) Seroepidemiology of Enterovirus 71 infection prior to the 2011 season in children in Shanghai. *J Clin Virol* 53:285–289
- Zhang W, Zhang L, Wu Z, Tien P (2014) Differential interferon pathway gene expression patterns in Rhabdomyosarcoma cells during Enterovirus 71 or Coxsackievirus A16 infection. *Biochem Biophys Res Commun* 447:550–555

Zhou J, Chng WJ (2013) Roles of thioredoxin binding protein (TXNIP) in oxidative stress, apoptosis and cancer. *Mitochondrion* 13:163–169

Zhou J, Bi C, Cheong LL, Mahara S, Liu SC, Tay KG, Koh TL, Yu Q, Chng WJ (2011) The histone methyltransferase inhibitor, DZNep, up-regulates TXNIP, increases ROS production, and targets leukemia cells in AML. *Blood* 118:2830–2839

Zhou L, He X, Gao B, Xiong S (2015) Inhibition of histone deacetylase activity aggravates coxsackievirus B3-induced myocarditis by promoting viral replication and myocardial apoptosis. *J Virol* 89:10512–10523